

PEROVSKITES

Thermal unequilibrium of strained black CsPbI₃ thin films

Julian A. Steele^{1*}, Handong Jin², Iurii Dovgaliuk³, Robert F. Berger⁴, Tom Braeckevelt⁵, Haifeng Yuan^{2,6}, Cristina Martin^{2,7}, Eduardo Solano⁸, Kurt Lejaeghere⁵, Sven M. J. Rogge⁵, Charlotte Notebaert⁹, Wouter Vandezande¹, Kris P. F. Janssen², Bart Goderis⁹, Elke Debroye², Ya-Kun Wang⁶, Yitong Dong⁶, Dongxin Ma⁶, Maksud Saidaminov⁶, Hairen Tan^{6,10}, Zhenghong Lu¹¹, Vadim Dyadkin³, Dmitry Chernyshov³, Veronique Van Speybroeck⁵, Edward H. Sargent⁶, Johan Hofkens^{2,*}, Maarten B. J. Roeflaers¹

The high-temperature, all-inorganic CsPbI₃ perovskite black phase is metastable relative to its yellow, nonperovskite phase at room temperature. Because only the black phase is optically active, this represents an impediment for the use of CsPbI₃ in optoelectronic devices. We report the use of substrate clamping and biaxial strain to render black-phase CsPbI₃ thin films stable at room temperature. We used synchrotron-based, grazing incidence, wide-angle x-ray scattering to track the introduction of crystal distortions and strain-driven texture formation within black CsPbI₃ thin films when they were cooled after annealing at 330°C. The thermal stability of black CsPbI₃ thin films is vastly improved by the strained interface, a response verified by ab initio thermodynamic modeling.

The use of solution-processed, organic-inorganic metal halide perovskites for solar cells (1–5) is still limited by their instability within real-world devices (6) for two reasons. The first relates to the volatility of organic cations in methylammonium and formamidinium (FA) lead halide systems, which promotes material degradation (7–9). The second arises from their polymorphic nature, whereby a room-temperature (RT) stable black perovskite structure is not guaranteed (10). Implementing Cs⁺ cations (i.e., CsPbI₃) has allowed for both high solar cell conversion efficiencies [above 17% (11)] and improved environmental stability (12, 13). However, regarding phase stability, single-cation FA/CsPbI₃ systems form a thermodynamically stable yellow RT δ -phase (nonperovskite) before

undergoing reversible, high-temperature phase transitions to their optically active black perovskite phases: α (cubic), β (tetragonal), and γ (orthorhombic). The thermal phase relations for CsPbI₃ are depicted in Fig. 1A, with the relative transitions shown in Fig. 1B. The term “black” is used to define collectively the (pseudo-)cubic phases, as they typically exhibit similar optoelectronic properties. At RT, the black phase is unstable (14, 15).

As seen in Fig. 1A, the black α -CsPbI₃ perovskite can, depending on conditions, pass through a variety of different restructuring paths. The thermodynamically preferred cooling path (path 2) (16) is mediated by the series of structural distortions (Fig. 1B). When the requisite sample preparation and cooling rates are used, an RT black phase can persist (paths 3 and 4 in Fig. 1A) in the form of a pseudocubic phase. A metastable black phase will only survive at RT when the strong driving force to transform into the yellow phase (path 5) is successfully countered. For example, upon mild reheating (60 to 100°C), the metastable black phase (path 6) will normally turn yellow (14, 15, 17) once its saddle point is energetically overcome. Thus, the problem is how to form a stable black CsPbI₃ perovskite for near-RT device operation.

Recent findings offer a range of solutions, each following at least one of three general approaches: (i) nanocrystal formation (18–21), (ii) surface functionalization (22), and (iii) compositional tuning (23–25). When forming a perovskite-substrate heterojunction in thin-film device architectures, tensile strain was recently shown to manifest at RT (26) due to the large mismatch in thermal expansion coefficients (α_T) of the perovskite layer ($\sim 50 \times 10^{-6} \text{ K}^{-1}$ for lead iodide-based perovskites) and typical optically transparent substrates [both indium tin oxide (ITO) and glass reside between

4×10^{-6} and $9 \times 10^{-6} \text{ K}^{-1}$]. By definition, strain will push the competing perovskite phases into a relative state of thermodynamic unequilibrium (27–29). Within this context, strain engineering can favor the formation of a desired phase or can even lead to new phases (30). For example, the strain introduced into CsPbI₃ nanocrystals processed with hydroiodic acid (29) has been connected to improved stability.

We report the use of interfacial clamping and strain to form an RT-stable black phase of functional CsPbI₃-based thin films. A combination of synchrotron-based, grazing incidence, wide-angle x-ray scattering (GIWAXS) and ab initio thermodynamic modeling revealed that substrate clamping drives texture formation (preferential alignment of domains within a polycrystalline system) and can create large biaxial strain. Strain beneficially shifted the relative free energies of the competing phases at RT. We elucidate the stabilizing roles of Br doping ($\leq 10\%$) and thin-film formation [i.e., nanocrystal (NC) formation and substrate clamping], and find that strain is a key enabler in the design of stable optoelectronic devices.

We grew CsPbI₃ materials using a solution-processing method previously reported (31), with the black phase accessed through thermal annealing (see the materials and methods). Three material types were considered: powders (drop cast), thin films (spin coat), and free NCs scraped from the thin-film substrate. Figure S1 presents scanning electron microscopy data showing their differing morphologies; the thin films exhibited the formation of NC grains (50 to 200 nm), and the powders appear bulk-like.

Synchrotron-based GIWAXS was used (see fig. S2 for experimental scheme) to resolve the structural state of a CsPbI₃ thin film before and after thermal annealing at 330°C, as well as after thermal quenching (i.e., kinetically trapping the black phase using an RT metal slab; path 3 in Fig. 1A). Figure S3 presents the structural refinements of a δ -CsPbI₃ thin film at RT and its α -phase (330°C), which is consistent with the result of Trots and Myagkota (32). A black phase was obtained at RT by kinetically trapping the thin film, hinting at the role of the interface for suppressing the α -to- δ phase transformation. In situ GIWAXS experiments showed that the strained black thin film remained vulnerable to moisture attack, quickly destabilizing and turning yellow when exposed to moisture (fig. S4). Figure 2A displays the GIWAXS image detected from a black γ -CsPbI₃ thin film shortly after quenching, highlighting occurrences of anisotropic peak splitting in-plane (q_{xy}) and out-of-plane (q_z) (fig. S5 shows the full GIWAXS image). This feature is a signature of crystallographic texture (preferential crystallographic orientation with distribution φ ; see fig. S6) in the quenched thin film, a signature not observed before or after gradual cooling (fig. S7). Figure 2B illustrates how this split GIWAXS signal arises after cooling; the CsPbI₃ lattice forming an interface is lengthened in-plane when clamped, corresponding to a relative lattice reduction out-of-plane.

¹Centre for Surface Chemistry and Catalysis, KU Leuven, Celestijnenlaan 200F, Leuven 3001, Belgium. ²Department of Chemistry, KU Leuven, Celestijnenlaan 200F, Leuven 3001, Belgium. ³Swiss-Norwegian Beamlines at the European Synchrotron Radiation Facility, 71 Avenue des Martyrs, F-38000 Grenoble, France. ⁴Department of Chemistry, Western Washington University, 516 High Street, Bellingham, WA 98225, USA. ⁵Center for Molecular Modeling (CMM), Ghent University, Technologiepark 46, 9052 Zwijnaarde, Belgium. ⁶Department of Electrical and Computer Engineering, University of Toronto, 35 St. George Street, Toronto, Ontario M5S 1A4, Canada. ⁷Departamento de Química Física, Facultad de Farmacia, Universidad de Castilla-La Mancha, 02071 Albacete, Spain. ⁸NCD-SWEET Beamline, ALBA Synchrotron Light Source, Cerdanyola del Vallès, Barcelona 08290, Spain. ⁹Polymer Chemistry and Materials, KU Leuven, Celestijnenlaan 200F, Leuven 3001, Belgium. ¹⁰National Laboratory of Solid State Microstructures, Jiangsu Key Laboratory of Artificial Functional Materials, College of Engineering and Applied Sciences, Nanjing University, Nanjing 210093, China. ¹¹Department of Materials Science and Engineering, University of Toronto, 184 College Street, Toronto, Ontario M5S 3G4, Canada.

*Corresponding author. Email: julian.steele@kuleuven.be (J.A.S.); johan.hofkens@kuleuven.be (J.H.)

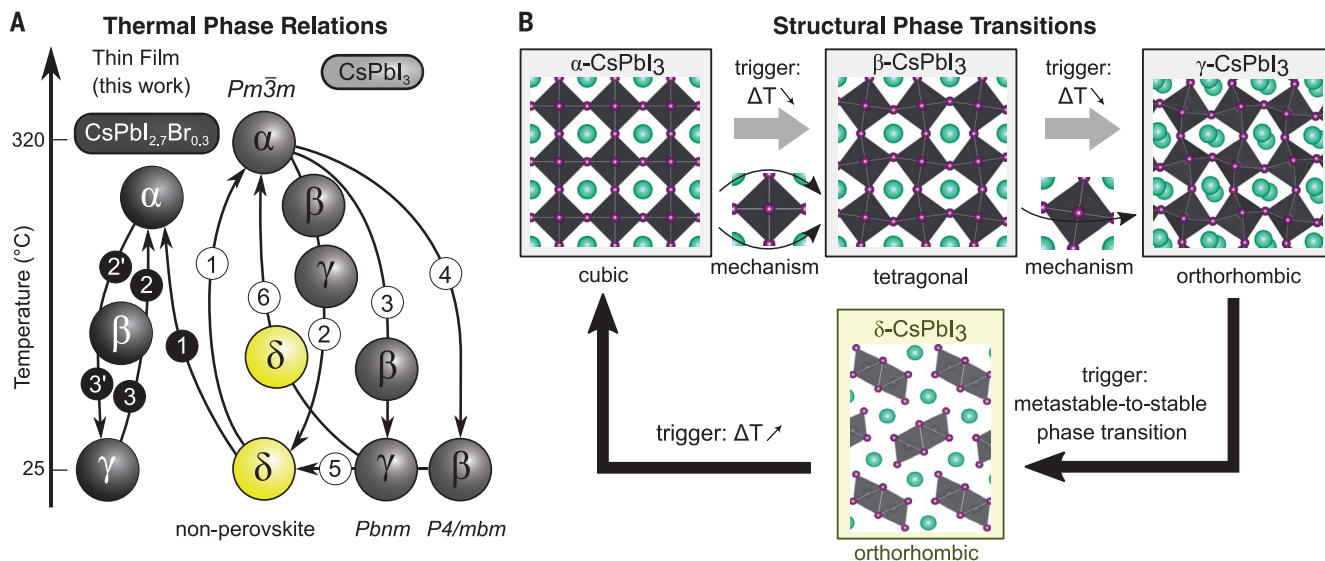


Fig. 1. Polymorphic character and metastability of CsPbI₃. (A) Thermal phase relations of CsPbI₃ compared with the phase behavior of strained CsPbI_{2.7}Br_{0.3} thin films investigated in this work. The different path details are outlined in the text. (B) Crystal structure of the different phases and

their relative phase transitions. The transitions between the black phases are governed by the local Pb-centered octahedral (black) distortions, depicted here using one lead atom at the center and six iodide atoms at the edges (purple), confining the cesium cations (cyan).

Figure 2C shows analysis of the 2θ scattering intensities generated along directions $q_{x,y,z}$, q_x , and $q_{x,y,z}$. Compared with the cubic α -phase (fig. S3), a reduction in crystal symmetry is evident from the more complex scattering pattern (16, 33). Refining the $q_{x,y,z}$ data (with the Le-Bail method) using a γ -CsPbI₃ structure (16) provided an agreeable fit and yielded unit cell parameters $a = 8.629 \text{ \AA}$, $b = 8.955 \text{ \AA}$, and $c = 12.636 \text{ \AA}$ (volume = 976.509 \AA^3). Analyzing the GIWAXS image pixel intensities in Fig. 2A as a function of the azimuthal angle, we were able to quantify the degree of texturing (fig. S8). We found that the intensity of the $\gamma(002)/(020)$ scattering peaks maximized in-plane, whereas the $\gamma(200)$ peak was normal to this. The $\gamma(110)$ peak exhibited an out-of-plane bimodal distribution (two maxima separated by $\sim 90^\circ$), with the full width at half maxima for both being near 55° , providing a measure of the orientational distribution, φ . An illustration of the crystal texture derived from this analysis is provided in fig. S9.

The texture was imposed by the symmetry of the initial high-temperature cubic unit cell. Any phase transition that results from a reduction in symmetry (forming an anisotropic cell) is paralleled by the formation of domains, e.g., a transition from a cubic (α) to a lower-symmetry tetragonal phase (β) gives three equally probable domains. In an isotropic bulk α -CsPbI₃ system, the domains have the same energy upon cooling and are equally probable. However, the situation changes after the introduction of an anisotropic strain field at the interface that energetically favors some domains, causing the longer lattice b - and c -axes to remain in-plane (fig. S8).

Compared with the bulk γ -CsPbI₃ structure refined by Marrognier *et al.* (16), our thin-film γ -CsPbI₃ crystal was heavily distorted (fig. S10)—

a result of clamping strain and rapidly cooling the material from 330°C down to RT on a glass substrate. In quantifying the extent of crystal deformation, we assessed distortions using the split low-angle peak(s) nearing $2\theta = 9^\circ$ (inset of Fig. 2C). These peaks arose during the α -to- γ transition through a relative doubling of the c -axis [i.e., $\alpha(001)$ becomes $\gamma(002)$] and a reduction in the unit-cell symmetry, whereby the (110) spacing is no longer equal to (002) in the pseudocubic β - or γ -phase. Considering the distortions in- and out-of-plane relative to the parent cubic, we evaluated the degree of biaxial anisotropy as follows:

$$\Delta d_{\perp} = 1 - \frac{d_{(110)}(q_z)}{d_{(001)}(q_{x,y})} \quad (1)$$

Here, d is the interplane spacing in the direction noted. Because of the relative transformation of the c -axis length during the α -to- γ transition, $d_{(001)}$ represents the normalized spacing. For a quenched RT black CsPbI₃ thin film, $\Delta d_{\perp} = 1.65\%$.

Two different types of strain act to increase the size of Δd_{\perp} : (i) spontaneous strain, which is introduced by a change in unit cell shape during the phase transition(s), and (ii) strain at the film/substrate interface, which is induced by the thermal expansion mismatch. Spontaneous strain can be decoupled from our measurement by using the temperature-dependent changes in the bulk CsPbI₃ lattice parameters, data recently reported by Marrognier *et al.* (16). By analyzing their data (see fig. S10), we found that Δd_{\perp} jumped to 1.18% during the α -to- β tetragonal distortion and ceased to increase after forming an orthorhombic γ -phase. The value $\Delta d_{\perp} = 1.18\%$ after the tetragonal distortion represents the spontaneous strain contribution of the RT γ -CsPbI₃

system, with an additional 0.47% arising in our thin film from substrate clamping. Thus, the effect of the interface is an out-of-plane structural relaxation of the same nature driven by the phase transitions (Fig. 1B), leading to texture formation and a continuation of the spontaneous strain and anisotropy.

To investigate whether the concept of strain-induced stabilization was a more general one, we explored the development of strain in the solution-processed thin films as a function of film thickness. With increasing thickness, the relative volume of the perovskite film that is subject to strain will decrease. The films shown in Fig. 2 were $\sim 270 \text{ nm}$ thick, so we varied the solution precursor concentration to prepare CsPbI₃ thin films with thicknesses ranging from 135 nm up to nearly $1 \mu\text{m}$ (an upper limit constrained by the solubility of precursor) and evaluated the structural state of their kinetically trapped RT black phase using GIWAXS (fig. S11). The strain profile and texture properties were consistent across the film thickness range studied. Further, Δd_{\perp} retained a value close to 1.65%, although it did decrease slightly to 1.62% for the thickest films (fig. S12). For devices based on solution-processed perovskite thin films, this suggests substrate clamping and the formation biaxial strain to be centrally important.

In a second stage, the properties of the thermodynamically preferred δ -phase material formation were investigated. A slowly cooled CsPbI₃ thin film ($-5^\circ\text{C}/\text{min}$) was tracked in situ (Fig. 1D) through an α -to- δ phase transition with GIWAXS time-temperature (t - T) profiling. The black-to-yellow phase change was identified by the introduction of δ peaks near 270°C and the fading of the black phase peak(s), which turn asymmetric with reduced crystallographic symmetry. The signals recorded in the $q_{x,y,z}$ and q_z directions are

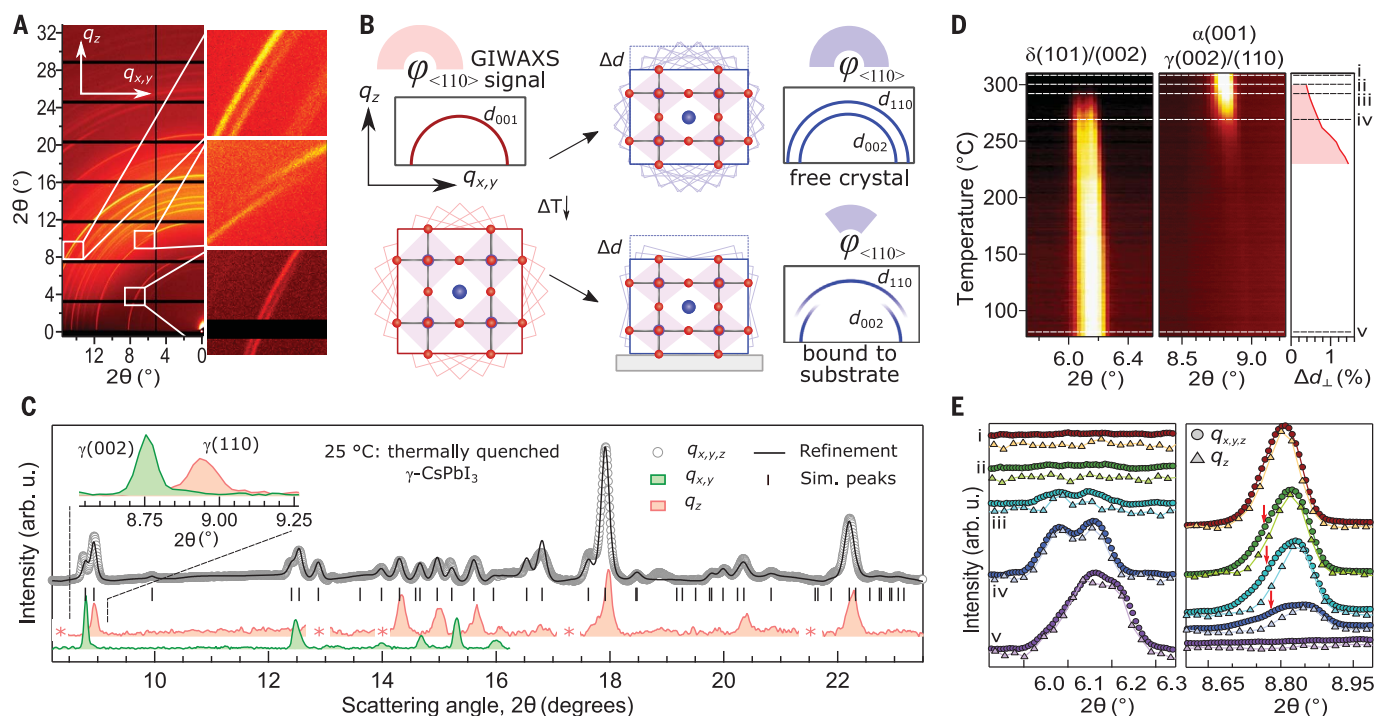


Fig. 2. Structural evaluation of substrate clamping and texture formation after the cooling of high-temperature α -CsPbI₃ thin films.

(A) GIWAXS image acquired from a thermally quenched RT CsPbI₃ thin film, with expansions over selected diffraction peaks azimuthally split in the in-plane ($q_{x,y}$) and out-of-plane (q_z) directions. (B) Schematic illustration of diffraction ring splitting in the GIWAXS signal, whereby a perovskite crystal forms a heterojunction with the substrate surface at high temperature and undergoes tensile strain and texture formation (with angular distribution φ , represented by light rotated cells) upon

cooling. (C) Comparison of GIWAXS 2θ signals generated from the image in (A), formulated by integrating over the total image ($q_{x,y,z}$) and both the $q_{x,y}$ and q_z directions. Asterisks indicate scattering blind spots between the cells of the detector. Inset is an expansion of the low-angle peaks. (D) GIWAXS t - T profile and calculated strain Δd_{\perp} (Eq. 1) through an α -to- δ phase transition in a slowly cooled ($-5^{\circ}\text{C}/\text{min}$) CsPbI₃ thin film. (E) Comparison of $q_{x,y,z}$ and q_z 2θ signals extracted at the points marked on the t - T profile in (D). The arrows identify the missing $q_{x,y}$ signal components detected in the $q_{x,y,z}$ direction, but not the q_z direction.

compared in Fig. 2E at the selected t - T values shown in Fig. 2D. Again, both strain and texture were established in the black phase during cooling, as seen by the distinct absence of $\gamma(110)$ scattering in $q_{x,y}$. Before the black phase disappeared, Δd_{\perp} increased throughout the phase change toward the expected spontaneous strain limit ($\sim 1.2\%$ for purely spontaneous strain; see fig. S10).

The introduction of the yellow phase in Fig. 2E underwent a contrasting evolution; the growth of δ -phase peaks upon cooling was paralleled by the loss of texture and strain within the polycrystalline thin film (fig. S7). This result indicates that a sharp and clamped interface was lost once the film transformed to the yellow phase through strain release (i.e., plastic deformation), facilitated by the near-equilibrium transformation kinetics above 200°C . The constraint of the perovskite atoms at the interface was the cause for this; if the atoms were to remain affixed during a δ -phase restructuring, then there would be an increased energy penalty. The black-to-yellow phase conversion involved a marked shift in the crystal volume (16) (per unit formula) and a total repositioning of atomic coordinates. The in situ XRD findings of Frolova *et al.* (15) visualized this directly; their [001]-oriented black films (grown

by vapor deposition) became disordered after a transition to the yellow phase. They also attributed the results to the large mismatch in the structure of different crystal phase layers relative to the substrate.

To investigate the influence of the strained interface on the relative stability of the α and δ phases, we monitored the local phase of a CsPbI₃ thin film that was partly scraped (forming free NCs), as it is thermally quenched from 330°C (Fig. 3A). From the optical images recorded in situ during the cooling ramp, the material that was still attached to the substrate became kinetically trapped at RT in the black phase, whereas the free NCs readily turned yellow below 230°C . This result confirmed the stabilizing role of the interface and its generated strain. To investigate whether the perovskite films respond in a similar way when clamped to other common interfaces, we evaluated the GIWAXS and phase behavior of CsPbI₃ thin films deposited on ITO-coated glass substrates (possessing a similar α_T value; see fig. S13). The root mean square roughness of the ITO (3.1 nm) is far larger than that of the bare glass (1.1 nm), yet the strain profile, crystal texture properties, and clamping-induced phase properties of thin films on the ITO surface are all comparable (fig. S13). This extends the influence of substrate

clamping and improved black-phase stability across substrates possessing different roughness and chemical natures, suggesting that such parameters are unimportant in establishing a strained interface or a stable black thin film.

To understand the strain-induced shifts in the energetic stability of the competing phases, periodic density functional theory (DFT) calculations of strained and unstrained γ - and δ -CsPbI₃ structures were performed (Fig. 3, B and C). Our approach (see the materials and methods) first considered the average unstrained linear reduction ($\overline{\Delta L}$) of the CsPbI₃ crystal when it was cooled to 100°C (where the black and yellow phases strongly compete energetically), which resulted in different degrees of relative contraction for γ and δ (16) (Fig. 3B). Our experiments revealed that the interface in the RT black phase prevented shrinking along the in-plane direction, heavily distorting the crystal. As a result, cooling from 300° to 100°C introduced an in-plane biaxial strain of $\sim 1\%$. Moreover, our DFT calculations using the SCAN (strongly constrained appropriately normed) functional (at 0 K) showed that the equilibrium volume per formula unit of δ -CsPbI₃ (229 \AA^3) was substantially less than that of the γ -CsPbI₃ (241 \AA^3), forcing the strain to grow to $\sim 3\%$ if the

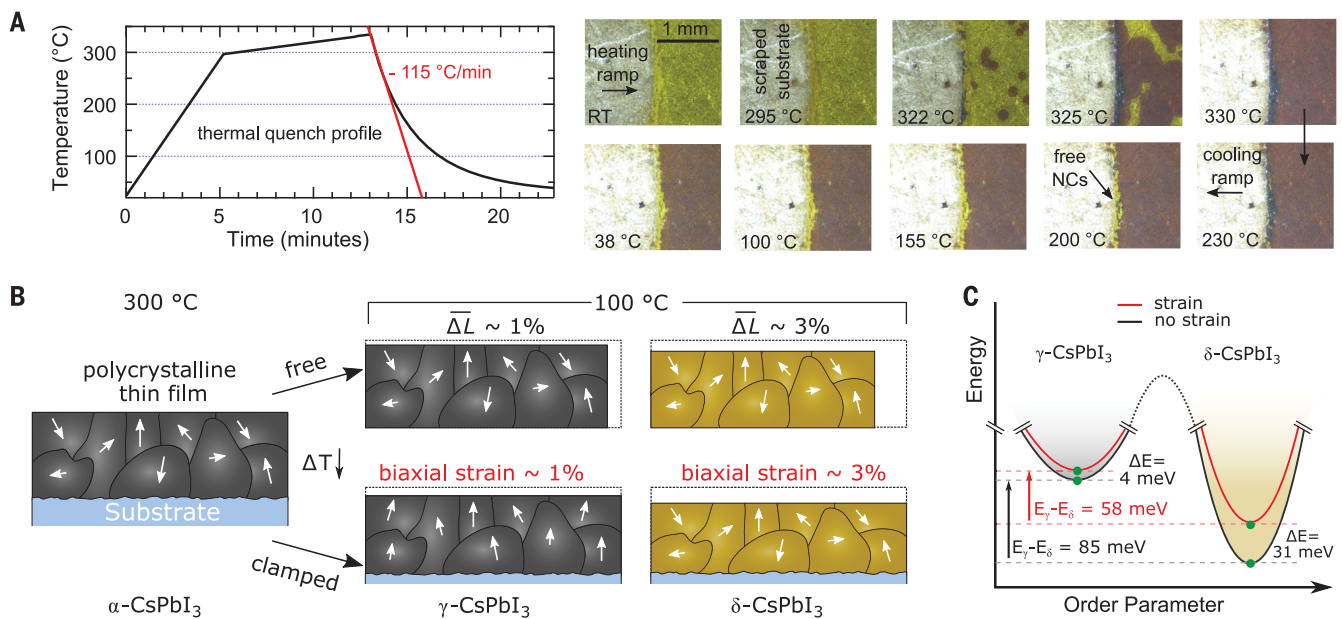


Fig. 3. Removing the interface destabilizes RT black CsPbI₃ thin films. (A) Corresponding optical images (right) of a partially scrapped CsPbI₃ thin-film surface (free NCs) recorded under N₂ at different temperatures during a quenching temperature profile (left). (B) Schematic representation of the DFT calculations used to quantify the energy of both the black γ -phase and yellow δ -phase materials that strongly compete at 100°C when cooled from the high-temperature α -CsPbI₃. The scenarios

considered include free and clamped polycrystalline thin films (arrows reflect relative domain orientation), where the thermal change induces a reduction in the average lattice parameter length ($\overline{\Delta L}$), manifesting as biaxial strain when clamped to the substrate. (C) Ab initio energy diagram indicating the relative stability (at 0 K) of the black and yellow phases with and without in-plane biaxial strain, averaged out over 12 different strain directions (see table S1). The relative saddle point depth is undefined.

material underwent a γ -to- δ phase transition while remaining clamped. The quenched γ -CsPbI₃ thin film was polycrystalline and expressed texture, whereas the crystallographic alignment was lost in the film upon transforming to the yellow phase. To account for this, 12 different crystal orientations were considered, resulting in 12 different strained interfacial planes, with the lower-symmetry planes forming supercells (fig. S14). Their energy increase upon straining is listed in table S1 and varied only slightly across the different surface orientations.

The average relative energies determined from periodic DFT simulations (Fig. 3C) show that the unstrained yellow phase is strongly favored over the unstrained black phase, driving the γ -to- δ phase transition in free-standing crystals. However, the introduction of biaxial strain led to different energy penalties for the two phases. There was a strong relative destabilization of the strained yellow phase with respect to the strained black phase. Thus, the energy difference promoting the γ -to- δ transition was reduced, explaining in part the stabilizing influence of substrate clamping that we saw experimentally. An additional energy penalty may be present if release of the surface clamping is required, as suggested by the kinetic trapping of the CsPbI₃ thin film.

We never formed an RT black-phase CsPbI₃ thin film without kinetic trapping, with the limited lifetime of the black phase during slow cooling (Fig. 2D) preventing a detailed study of the strain-induced restructuring. For this, we used relatively light Br halide mixing to better access the

temperature-dependent black-phase evolution, i.e., CsPb(I_{1-x}Br_x)₃, $x \leq 0.1$. These materials retain both a band-gap energy useful for solar cells (fig. S15) and comparable material morphologies (fig. S1).

Differential scanning calorimetry (DSC) studies of CsPb(I_{1-x}Br_x)₃ powders and NCs (fig. S16) provided two pertinent types of data. First, size-driven effects likely make the NCs formed during spin coating more stable than the bulk materials. A disparity in the surface energy between γ -CsPbI₃ (0.13 J/m²) and δ -CsPbI₃ (2.57 J/m²) is predicted (21) to reverse the relative magnitudes of their Gibbs free energies at crystal volumes approaching ~ 100 nm³. The size of nanograins making up our thin films (fig. S1) was near this regime. Second, although Br doping helped to stabilize the black phase, the calculated enthalpies (table S2) of the reversible yellow-to-black phase transitions were comparable (13 kJ/mol) and steady across the Br mixing explored. This result suggests that the phase transitions in our mixed halide samples closely followed the thermodynamics of the parent CsPbI₃ system.

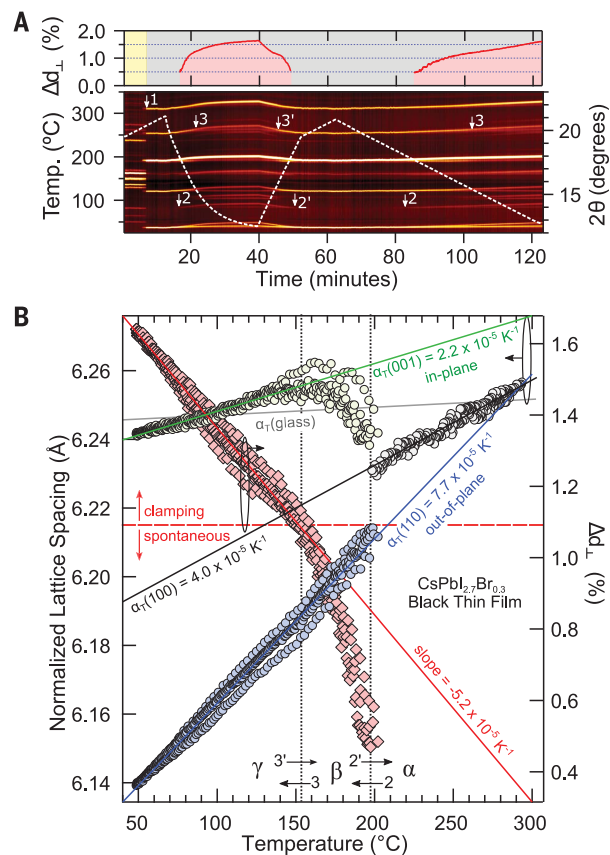
Figure 4A shows the GIWAXS t - T profile and strain state in a CsPbI_{2.7}Br_{0.3} thin film through multiple phase transitions imposed during thermal cycling. The changes therein can be tracked after the successive phase transitions, whereas the emergence of texture induced by anisotropic strain results in azimuthal splitting; the latter effect can only be seen with a large area detector. Starting from δ -CsPbI_{2.7}Br_{0.3}, we saw the high-temperature formation of the α -phase (1), followed by β (2) and γ (3) distortion during cooling,

which were reversed (2' and 3') upon reheating. After an initial yellow-to-black transition, a thermodynamically stable black thin film with a strained interface was realized. This is in contrast to the unstable free NCs studied by DSC (fig. S16), which do not benefit from the stabilizing strained interface. For completeness, the sequence described above for thin-film CsPbI_{2.7}Br_{0.3} was compared with the nominal thermal phase relations of CsPbI₃ in Fig. 1A. The textured GIWAXS signal (full image shown in fig. S17) and the crystal structure of the RT γ -CsPbI_{2.7}Br_{0.3} thin film is analogous to the quenched black CsPbI₃ thin film (fig. S4). The magnitude of Δd_L in the γ -CsPbI_{2.7}Br_{0.3} thin film at RT reached 1.64%, and reheating caused the strain-driven texture to be undone, reforming randomly distributed α -phase domains (see fig. S18). Thus, in addition to hindering a decay to the δ -phase (fig. S16), kinetically trapping a black CsPbI₃ thin film incurred no additional structural modification.

A temperature-domain structural analysis of the black CsPbI_{2.7}Br_{0.3} thin film (Fig. 4B) showed no considerable hysteresis between the different restructuring pathways (fig. S19). We thus evaluated these data together; as the temperature difference (ΔT) increased, the interplanar distances d shifted relative to $d_0(\Delta T = 0)$ by $d = d_0(1 + \alpha_T \times \Delta T)$. Linear fits yielded the α_T values shown in Fig. 4B using high-temperature d_0 values. Upon cooling the black film from 300°C, the lattice a -axis contracted smoothly with an expansion rate comparable (32) to the high-temperature α -CsPbI₃ ($\alpha_T = 4.0 \times 10^{-5} \text{ K}^{-1}$). Near 200°C, the cubic

Fig. 4. Structural phase kinetics of thermally cycled strained perovskite thin film. (A) GIWAXS ($\lambda = 0.95774 \text{ \AA}$) t - T profile ($q_{x,y,z}$) of CsPbI_{2.7}Br_{0.3} thin film through a high-temperature yellow-to-black phase transition, followed by thermal cycling. The start of the first cooling ramp (nonlinear) is $\sim -17^\circ\text{C}/\text{min}$ and the second is $-3.8^\circ\text{C}/\text{min}$.

(B) Normalized anisotropic lattice parameters and Δd_{\perp} unit cell distortions of the black phase thin film as a function of temperature. Phase changes are numerically identified in (B) and align with those depicted in (A). The linear data fits to selected segments generate the α_T values displayed. An estimate is provided for the thermal expansion of the glass substrate (35) ($\alpha_T = 0.37 \times 10^{-5} \text{ K}^{-1}$).



structure underwent a tetragonal distortion and the introduction of Δd_{\perp} through spontaneous strain formation. The in-plane (001) lattice underwent negative thermal expansion, reverting this in-plane lattice closer to the linear expansion rate of glass. The negative thermal expansion of the c -axis in this temperature range agreed well with the complex bulk structural evolution detailed by Marronnier *et al.* (16) (see fig. S10 for full analysis) and underpinned the subsequent texture direction. Cooling through point 3 in Fig. 4B, the out-of-plane lattice continued its relatively fast reduction, whereas the in-plane spacing of the orthorhombic structure assumed positive thermal expansion [compensated by negative thermal expansion of the b -axis (16); see fig. S10]. After the β -to- γ transition, Δd_{\perp} should not increase in a nonstrained system. In our clamped thin film, Δd_{\perp} grew rapidly and overshoot spontaneous strain contributions, being driven solely by the strained interface. With rising strain, the relative destabilization of the yellow phase was only expected to continue.

The small divergence of the in-plane CsPbI₃ lattice parameter (crystal c -axis) from the expected linear contraction of the glass suggests that the perovskite/substrate interface resulted from the adaptable nature of the perovskite crystal rather than from covalent bonding. This is supported by our studies of strained films deposited on ITO-covered glass (S13). The strong mirroring of the structural evolutions during thermal cycling signified high elastic recovery. Clamping and interfacial strain combined as key driving forces in

defining both the structural texture and the improved thermal phase relations of the black phase. Thus, once a δ -CsPbI_{2.7}Br_{0.3} thin film was annealed at high temperatures, it became thermodynamically trapped in an optically active black phase (Fig. 1A). Such thermal stability is highly desirable within optoelectronic devices; for instance, the energy provided by a light-emitting diode (LED)-driving current can readily destabilize the black phase (34). As a conceptual demonstrator, we fabricated and characterized a functioning LED device using a strained CsPbI_{2.7}Br_{0.3} active layer (see fig. S20 for full details). Without any optimization, the result is a working LED device with a visibly bright (luminance of 20 cd/m² at 9 V) and high color purity (CIE coordinates: 0.72, 0.28) emission.

REFERENCES AND NOTES

- M. A. Green, A. Ho-Baillie, H. J. Snaith, *Nat. Photonics* **8**, 506–514 (2014).
- P. Meredith, A. Armin, *Nat. Commun.* **9**, 5261 (2018).
- S. D. Stranks *et al.*, *Science* **342**, 341–344 (2013).
- A. Walsh, A. Zunger, *Nat. Mater.* **16**, 964–967 (2017).
- S. I. Seok, M. Grätzel, N.-G. Park, *Small* **14**, e1704177 (2018).
- Y. Yang, J. You, *Nature* **544**, 155–156 (2017).
- J. A. Christians, P. A. Miranda Herrera, P. V. Kamat, *J. Am. Chem. Soc.* **137**, 1530–1538 (2015).
- B. Conings *et al.*, *Adv. Energy Mater.* **5**, 1500477 (2015).
- G. E. Eperon *et al.*, *Energy Environ. Sci.* **7**, 982 (2014).
- J. A. Christians, S. N. Habisreutinger, J. J. Berry, J. M. Luther, *ACS Energy Lett.* **3**, 2136–2143 (2018).
- Y. Wang, T. Zhang, M. Kan, Y. Zhao, *J. Am. Chem. Soc.* **140**, 12345–12348 (2018).
- M. Kulbak, D. Cahen, G. Hodes, *J. Phys. Chem. Lett.* **6**, 2452–2456 (2015).
- J. Liang *et al.*, *J. Am. Chem. Soc.* **138**, 15829–15832 (2016).

- S. Dastidar *et al.*, *J. Phys. Chem. Lett.* **8**, 1278–1282 (2017).
- L. A. Frolova *et al.*, *J. Phys. Chem. Lett.* **8**, 67–72 (2017).
- A. Marronnier *et al.*, *ACS Nano* **12**, 3477–3486 (2018).
- T. Burwig, W. Franzel, P. Pistor, *J. Phys. Chem. Lett.* **9**, 4808–4813 (2018).
- D. Zhang *et al.*, *J. Am. Chem. Soc.* **138**, 13155–13158 (2016).
- Y. Wang *et al.*, *Adv. Mater.* **27**, 7101–7108 (2015).
- A. Swarnkar *et al.*, *Science* **354**, 92–95 (2016).
- B. Zhao *et al.*, *J. Am. Chem. Soc.* **140**, 11716–11725 (2018).
- Y. Fu *et al.*, *Nano Lett.* **17**, 4405–4414 (2017).
- M. Lu *et al.*, *ACS Energy Lett.* **3**, 1571–1577 (2018).
- Y. Hu *et al.*, *ACS Energy Lett.* **2**, 2219–2227 (2017).
- Z. Li *et al.*, *Chem. Mater.* **28**, 284–292 (2016).
- J. Zhao *et al.*, *Sci. Adv.* **3**, eaao5616 (2017).
- K. M. Rabe, U. V. Waghmare, *Ferroelectrics* **194**, 119–134 (1997).
- F. He *et al.*, *Phys. Rev. B Condens. Matter Phys.* **70**, 23405 (2004).
- G. E. Eperon *et al.*, *J. Mater. Chem. A Mater. Energy Sustain.* **3**, 19688–19695 (2015).
- Y. Cao *et al.*, *J. Phys. Chem. C* **122**, 9332–9338 (2018).
- R. E. Beal *et al.*, *J. Phys. Chem. Lett.* **7**, 746–751 (2016).
- D. M. Trots, S. V. Myagkota, *J. Phys. Chem. Solids* **69**, 2520–2526 (2008).
- R. J. Sutton *et al.*, *ACS Energy Lett.* **3**, 1787–1794 (2018).
- Q. Shan *et al.*, *Small* **13**, 1701770 (2017).
- V. Craciun, D. Craciun, X. Wang, T. J. Anderson, R. K. Singh, *J. Optoelectron. Adv. Mater.* **5**, 401–408 (2003).

ACKNOWLEDGMENTS

Funding: The authors acknowledge financial support from the Research Foundation-Flanders (FWO, grant nos. G.0B39.15 and G098319N); FWO postdoctoral fellowships to J.A.S., C.M., H.Y., K.P.F.J., E.D., K.L., and S.M.J.R. (grant nos. 12Y7218N, 12J1716N, 12R8718N, 12C2817N, 12O3719N, 12O0117N, and 12T3519N, respectively); and an SB-FWO fellowship to T.B. (grant no. 15C1319); the KU Leuven Research Fund (C14/15/053); the Flemish government through long-term structural funding Methusalem (CASAS2, Meth/15/04); the Hercules Foundation (HER/11/14); and the Belgian Federal Science Policy Office (IAP-VII/05). The research leading to these results has received funding from the European Research Council under the European Union's Seventh Framework Programme (FP/2007-2013)/ERC Grant Agreement (grant no. 307523 LIGHT). E.S. is grateful for the GIWAXS experimental time provided by the NCD-SWEET beamline at ALBA synchrotron. T.B. and V.V.S. acknowledge funding from the European Union's Horizon 2020 research and innovation program (consolidator ERC grant agreement no. 647755 – DYNPOR, 2015–2020). V.V.S. acknowledges the Research Board of Ghent University (BOF). The computational resources and services used were provided by Ghent University (Stevin Supercomputer Infrastructure) and the VSC (Flemish Supercomputer Center), funded by FWO. **Author contributions:** J.A.S. conceived the science, coordinated the research, and wrote the manuscript under the supervision of J.H. and M.B.J.R. I.D., V.D., W.V., K.P.F.J., E.S., and D.C. assisted with the x -ray scattering experiments and analysis. H.J., H.Y., E.H.S., and E.D. synthesized the materials under investigation, and C.M., Y.-K.W., Y.D., D.M., and Z.L. prepared and characterized the LED devices. T.B. performed the DFT calculations under supervision of S.M.J.R., K.L., and V.V.S., with support from R.F.B. C.N. and B.G. performed the DSC experiments, and M.S. and H.T. assisted in developing the science. All authors have approved the manuscript.

Competing interests: The authors declare no competing financial interests. **Data and materials availability:** All data needed to evaluate the conclusions in this manuscript are present in the main text or the supplementary materials. Additional data or codes are available upon request to the corresponding authors. The commercial VASP software code can be licensed from the University of Vienna (see FAQ section on <https://www.vasp.at>). A patch with the user modifications in this article (to allow constrained cell optimizations) can be obtained from the authors upon request by VASP license holders.

SUPPLEMENTARY MATERIALS

science.sciencemag.org/content/365/6454/679/suppl/DC1
Materials and Methods
Figs. S1 to S20
Tables S1 and S2
References (36–42)

20 March 2019; accepted 10 July 2019
Published online 25 July 2019
10.1126/science.aax3878

Thermal unequilibrium of strained black CsPbI₃ thin films

Julian A. Steele, Handong Jin, Iurii Dovgaliuk, Robert F. Berger, Tom Braeckvelt, Haifeng Yuan, Cristina Martin, Eduardo Solano, Kurt Lejaeghere, Sven M. J. Rogge, Charlotte Notebaert, Wouter Vandezande, Kris P. F. Janssen, Bart Goderis, Elke Debroye, Ya-Kun Wang, Yitong Dong, Dongxin Ma, Makhsud Saidaminov, Hairen Tan, Zhenghong Lu, Vadim Dyadkin, Dmitry Chernyshov, Veronique Van Speybroeck, Edward H. Sargent, Johan Hofkens and Maarten B. J. Roelofs

Science **365** (6454), 679-684.

DOI: 10.1126/science.aax3878 originally published online July 25, 2019

Strain-stabilized perovskites

The perovskite materials used for solar cells and light-emitting diodes (which are black in color) are generally less stable at room temperature than the electronically inactive nonperovskite phases (which are yellow in color). Steele *et al.* show that for CsPbI₃, strain induced in a thin film after annealing the material to 330°C and then rapidly cooling it to room temperature kinetically trapped the black phase. Grazing-incidence wide-angle x-ray scattering revealed the crystal distortions and texture formation created by interfacial strain.

Science, this issue p. 679

ARTICLE TOOLS

<http://science.sciencemag.org/content/365/6454/679>

SUPPLEMENTARY MATERIALS

<http://science.sciencemag.org/content/suppl/2019/07/24/science.aax3878.DC1>

REFERENCES

This article cites 42 articles, 3 of which you can access for free
<http://science.sciencemag.org/content/365/6454/679#BIBL>

PERMISSIONS

<http://www.sciencemag.org/help/reprints-and-permissions>

Use of this article is subject to the [Terms of Service](#)